2.3 Top Quark Physics

The stage for the future of top physics has been set by the recent discovery [8] of top at Fermilab. The very large top mass, $m_t \approx 174 \pm 8$ GeV/c^2, forces one to consider the possibility that the top quark plays a special role in particle physics. At the very least, the properties of the top quark could reveal important information about the physics of electroweak symmetry breaking. In this context, the determination of the complete set of top quark properties should be an important goal. A high-energy future linear e^+e^- collider provides a very impressive tool to carry out a detailed top quark physics program.

The $t\bar{t}$ threshold region has a rich phenomenology which derives from its mix of toponium and continuum structure. Only in e^-e^+ collisions can this threshold structure be properly resolved, making possible definitive measurements of the top mass and width and tests of the QCD potential at very short range. Above threshold, the NLC makes it possible to measure the complete set of top couplings to gauge bosons, both for neutral current (γ and Z^0) and charged current interactions. The high electron-beam polarization available at NLC plays an important role in such studies, simplifying the search for anomalous top couplings and CP violating effects. A complete understanding of electroweak symmetry breaking will require the measurement of the Higgs boson couplings to fermions; of these, the coupling to top is the most accessible. At the NLC, this quantity can be measured by direct $t\bar{t}H$ production above threshold and also, if the Higgs boson is light, by the effect of Higgs boson exchange on the threshold properties. Finally, the NLC provides a relatively clean final state and precise vertex detection which make it straightforward to study the decays of the top. All standard decay modes can be reconstructed with reasonable efficiency, and exotic decay modes, in those examples studied to date, can be readily identified.

The physics program for the top quark also imposes important constraints on the NLC design. The energy must be adjustable, to run both at the $t\bar{t}$ threshold and at a point in the continuum about 100 GeV above threshold. The study of the threshold region requires that the center-of-mass energy spread be much smaller than the top quark width, and that tails in the energy distribution be understood. Experimenters must be able to determine both the absolute energy and the differential luminosity spectrum.

2.3.1 Top Production, Decay, and Measurement

The large mass of the top quark causes it to have a very large decay width, and this exerts a decisive influence on its phenomenology. In the Standard Model, the weak decay of top proceeds very rapidly via $t \to bW$, resulting in a total decay width given by

$$\Gamma_t \approx (0.18)(m_t/m_W)^3 \text{ GeV} . \tag{2.3}$$

For $m_t = 180$ GeV/c^2 this lowest-order prediction is $\Gamma_t = 1.71$ GeV. After first-order QCD and electroweak corrections [9], this becomes 1.57 GeV. Hence, top decay is much more rapid than the characteristic time for hadron formation, for which the scale is $\Lambda_{\rm QCD}$. This implies that the phenomenology of top physics is fundamentally different than that of the lighter quarks. For example, there will be no top-flavored mesons. While we lose the familiar study of the spectroscopy of these states, we gain unique clarity in the ability to reconstruct the properties of the elementary quark itself. This may prove to be a crucial advantage toward uncovering fundamental issues.

The top decay also provides a natural cutoff for gluon emission. Indeed, in $t\bar{t}$ processes, the nonperturbative color strings appear in fragmentation only after the tops decay and form along the separating b and $\bar{b}$ lines. Hard gluons emitted from the top and its product bottom quark can exhibit interference phenomena which are sensitive to the value of Γ_t [10, 11].

In the Standard Model, $|V_{tb}| \approx 1$, so that the decay mode $t \to bW$ completely saturates the decay width. Then the branching ratios are determined by the W decay modes from the $b\bar{b}W^+W^-$ intermediate state. This gives 6-jet, 4-jet + lepton, and 2-lepton final states in the ratio 4:4:1, or, including QCD corrections to the W decay rates, $\mathrm{BR}(t\bar{t} \to b\bar{b}qq'qq') = 0.455$; $\mathrm{BR}(t\bar{t} \to b\bar{b}qq'\ell\nu) = 0.439$; $\mathrm{BR}(t\bar{t} \to \ell\nu\ell\nu) = 0.106$, where $q = u, c$, $q' = d, s$, and $\ell = e, \mu, \tau$.

The parton-like decay of top implies that, unlike other quarks, its spin is transferred to a readily reconstructable final state. Measurement of the $b\bar{b}W^+W^-$ final state therefore provides a powerful means of probing new physics manifested by top with helicity analyses. This is explored in Section 2.3.3. Another implication of the large m_t is the Standard Model prediction that the decay $t \to bW$ produces mostly longitudinally polarized W bosons; the degree of longitudinal polarization is given by $m_t^2/(m_t^2 + 2m_W^2) \approx 72\%$ for $m_t = 180$ GeV/c^2. This reflects the fact that the longitudinally polarized W bosons contain degrees of freedom from the electroweak symmetry breaking sector.

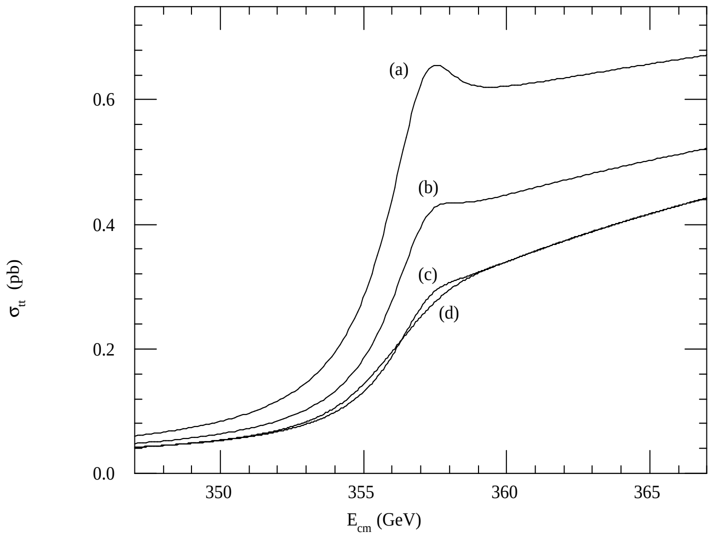

Figure 2.6: Production cross section for top-quark pairs near threshold for $m_t = 180$ GeV/c^2. The ideal theoretical cross section is given by curve (a). In curves (b), (c) and (d), we add, successively, the effects of initial-state radiation, beamstrahlung, and beam energy spread.

The $t\bar{t}$ cross section due to s-channel e^+e^- annihilation mediated by γ, Z bosons increases abruptly just below threshold (see Fig. 2.6), reaches a maximum at roughly 50 GeV above threshold, then falls roughly proportional to the point cross section, Eq. 2.2, as the energy increases. At $\sqrt{s} = 500$ GeV the lowest-order total cross section for unpolarized beams is 0.54 pb; it is 0.74 (0.34) for a fully left-hand (right-hand) polarized electron beam. Hence, in a design year of integrated luminosity (50 fb^{-1}) at $\sqrt{s} = 500$ GeV we can produce $25,000$ $t\bar{t}$ events. The cross sections for t-channel processes, resulting, for example, in final states such as $e^+e^-t\bar{t}$ or $\nu\bar{\nu}t\bar{t}$, increase with energy, but are still relatively small. We will discuss these processes in Section 7.3.

The emphasis of most event selection strategies has been to take advantage of the multi-jet topology of the roughly 90% of $t\bar{t}$ events with 4 or 6 jets in the final state. Therefore, cuts on thrust or number of jets drastically reduces the light fermion pair background. In addition, one can use the multi-jet mass constraints $M(\text{jet-jet}) \approx m_W$ and $M(\text{3-jet}) \approx m_t$. Simulation studies [12] have shown that multi-jet resolutions of 5 GeV/c^2 and 15 GeV/c^2 for the 2-jet and 3-jet masses, respectively, are adequate and readily achievable with LEP/SLC detectors. A detection efficiency of about 70% with a signal to background ratio of 10 was attained by selecting 6-jet final states just above threshold. These numbers are typical also for studies which select the 4-jet+$\ell\nu$ decay mode.

Of the backgrounds considered in this study, that from W-pair production is the most difficult to eliminate. However, in the limit that the electron beam is fully right-hand polarized, the W^+W^- cross section is dramatically reduced. Thus it is possible to use the beam polarization to experimentally control and measure the background. We note, though, that the signal is also somewhat reduced by running with a right-handed polarized beam. A possible strategy might be to run with a right-handed polarized beam only long enough to make a significant check of the background due to W pairs. Another important technique is that of precision vertex detection. The present experience with SLC/SLD can be used as a rather good model of what is possible at NLC. The small and stable interaction point, along with the small beam sizes and bunch timing, make the NLC ideal for pushing the techniques of vertex detection. This has important implications for top physics. Rather loose b-tagging, applied in conjunction with the standard topological and mass cuts mentioned above, should lead to substantially improved top event selection efficiencies and purities.

2.3.2 Threshold Physics

In Fig. 2.6 we show the cross section for $t\bar{t}$ production as a function of nominal center-of-mass energy for $m_t = 180$ GeV/c^2. In this discussion, m_t is the pole mass in QCD perturbation theory. The theoretical cross section, indicated as curve (a), is based on the results of Strassler and Peskin [13], using the $q\bar{q}$ potential of QCD with $\alpha_s(M_Z^2) = 0.12$ and Standard Model couplings to γ and Z. To this curve, the energy-smearing mechanisms of initial-state radiation, beamstrahlung, and beam energy spread, have been successively applied; curve (d) includes all effects. The beam effects were calculated using NLC design parameters.

The threshold enhancement given by the predicted cross section curve of Fig. 2.6a reflects the Coulomb-like attraction of the produced $t\bar{t}$ state due to the short-distance QCD potential

$$V(r) \sim -C_F \frac{\alpha_s(\mu)}{r} \ , \tag{2.4}$$

where $C_F = 4/3$ and μ is evaluated at the scale of the Bohr radius of this toponium atom: $\mu \sim \alpha_s m_t$. The level spacings of the QCD potential, approximately given by the Rydberg energy, $\sim \alpha_s^2 m_t$, turn out to be comparable to the widths of the resonance states, given by $\Gamma_\theta \approx 2\Gamma_t$. Thus, the bound state exists, on average, only for approximately one classical revolution before one of the top quarks undergoes a weak decay. The level spacings of the QCD potential approximately given by the Rydberg energy, $\sim \alpha_s^2 m_t$, turn out to be comparable to the widths of the resonance states, given by $\Gamma_\theta \approx 2\Gamma_t$. Therefore the various toponium states become smeared together, as seen in Fig. 2.6, where only the bump at the position of the 1S resonance is distinguishable. The infrared cutoff imposed by the large top width also implies [14] that the physics is independent of the long-distance behavior of the QCD potential. The assumed intermediate-distance potential is also found [12] to have a negligible impact. Hence, the threshold physics measurements depend only on the short-distance potential (Eq. 2.4) of perturbative QCD.

An increase of α_s deepens the QCD potential, thereby increasing the wave function at the origin and producing an enhanced 1S resonance bump. In addition, the binding energy of the state varies roughly as the Rydberg energy $\sim \alpha_s^2 m_t$. So the larger α_s has the combined effect of increasing the cross section as well as shifting the apparent position of the threshold to lower energy. The latter effect is also what is expected for a shift to lower m_t. Therefore, there exists a significant correlation between the measurements of α_s and m_t from a threshold scan.

A number of studies have been carried out to simulate the measurement of the $t\bar{t}$ threshold cross section. Figure 2.7a depicts a threshold scan [12] for which an integrated luminosity of 1 fb^{-1} has been expended at each of 10 energy points across the threshold, plus one point below threshold to measure backgrounds. A value of $m_t = 150$ GeV/c^2 was used. No beam polarization was assumed. A fit of the data points to the theoretical cross section, including all radiative and beam effects discussed above, results in a sensitivity for the measurement of m_t and α_s shown in Fig. 2.7b. The correlation between these two parameters is apparent. Even for the modest luminosity assumed here, the cross section measurement gives quite good sensitivity to these quantities. If no prior knowledge is assumed, the errors for m_t and α_s are 200 MeV/c^2 and 0.005, respectively. Conversely, the single-parameter sensitivity for m_t approaches 100 MeV/c^2 if α_s is known to much better than 2% accuracy. We will describe a method for the precision measurement of α_s in Section 10.1. The theoretical systematic error due to uncertainties in the $t\bar{t}$ threshold cross section is of order 200 MeV.

For a quarkonium state, we expect the cross section at the 1S peak to vary with the total width roughly as $\sigma_{1S} \sim |V_{tb}|/\Gamma_t$, and therefore is very sensitive to the width, as indicated in Fig. 2.8 for rather wide variations in Γ_t relative to the Standard Model expectation. (It is noted that the calculations of Figs. 2.6 and 2.8 use the uncorrected top width, so that the

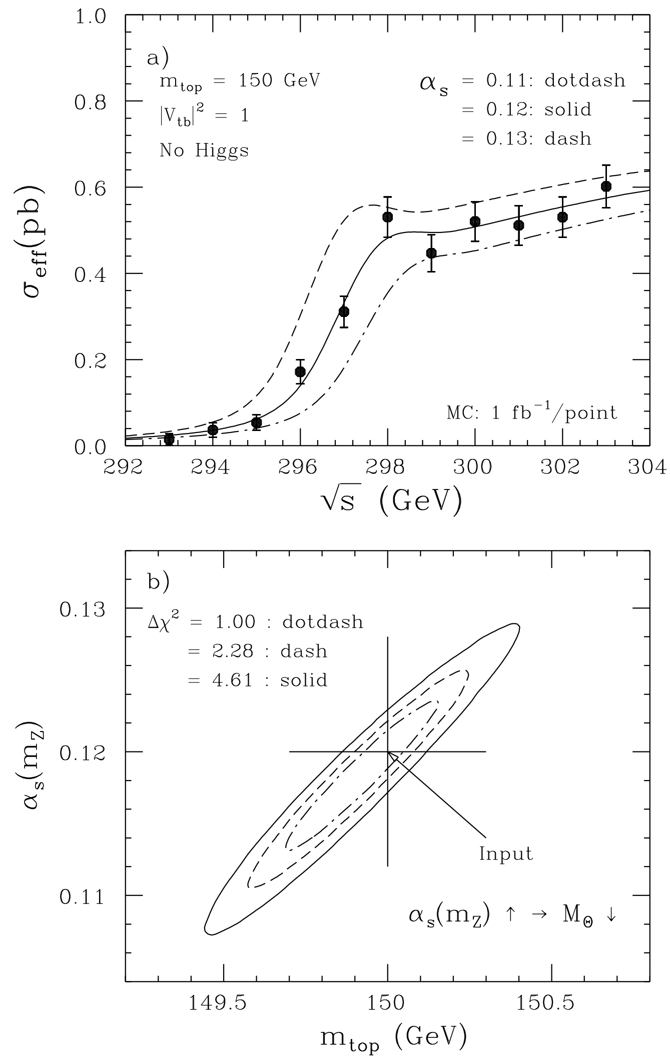

Figure 2.7: (a) Top threshold scan; (b) corresponding error ellipse for m_t and α_s. A value for m_t of 150 GeV/c^2 was assumed.

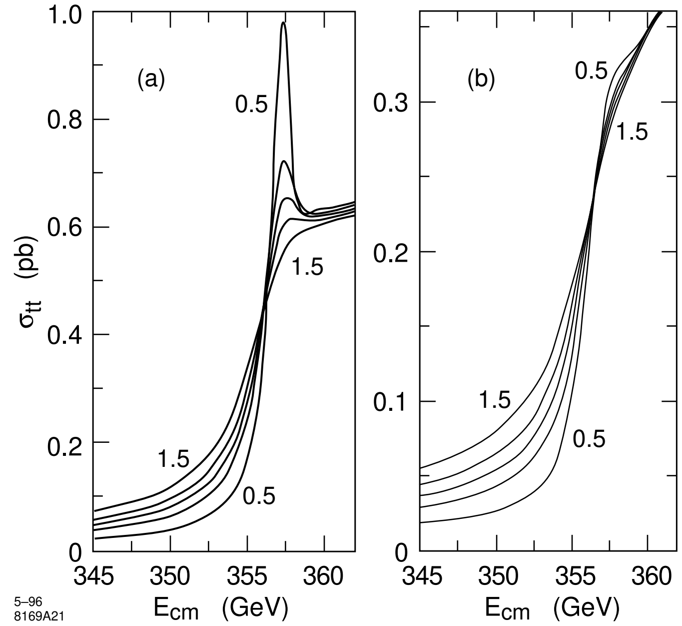

Figure 2.8: Variation of the $t\bar{t}$ threshold cross section with the top width for $m_t = 180$ GeV/c^2. The curves correspond to values of Γ_t/Γ_{SM} of 0.5, 0.8, 1.0, 1.2, and 1.5, presented in the order indicated, for (a) the theoretical cross section, and (b) the cross section after including radiative and beam effects.

resonance structure will be slightly more pronounced than what is shown.) After applying a correction for initial-state radiation and the beam-related energy spread, the width is affected as shown in Fig. 2.8. This implies that a scan strategy optimized for measuring Γ_t would spend a relatively large fraction of running time below the 1S peak. The threshold physics, combining the cross section information with the momentum and asymmetry results, as discussed below, represents what is most likely the best opportunity to measure Γ_t.

In addition to the QCD potential, the t-$\bar{t}$ pair is also subject to the Yukawa potential associated with Higgs exchange:

$$V_Y = -\frac{\lambda^2}{4\pi}\,\frac{e^{-m_H r}}{r}\ , \tag{2.5}$$

where m_H is the Higgs mass and λ is the $t\bar{t}$-Higgs Yukawa coupling, $\lambda = m_t/v = [\sqrt{2}G_F]^{1/2}\,m_t$. Because of the extremely short range of the Yukawa potential, its effect is primarily to alter the wave function at the origin, and hence to shift the level of the cross section. This exciting possibility is discussed further in Section 2.3.4. The physics of the threshold cross section is, in summary, expected to depend on the following set of parameters:

$$\sigma = \sigma(m_t, \alpha_s, \Gamma_t, m_H, \lambda)\ . \tag{2.6}$$

As we have discussed, the lifetime of the toponium resonance is determined by the first top quark to undergo weak decay, rather than by the annihilation process. This has the interesting implication that the kinetic energy (or momentum) of the top quark as reconstructed from its decay products reflects the potential energy of the top in the QCD potential. Hence, a measurement of the momentum distribution will be sensitive to α_s and Γ_t. The theory [15] and phenomenology [12, 16] of this physics has been extensively studied. A convenient observable which has been used to characterize the distribution is the position of the peak in the reconstructed top quark momentum distribution. The position of this peak at a given center-of-mass energy is indeed found to be sensitive to Γ_t and the other parameters in Eq. 2.6.

Yet another, quite different observable has been studied [17, 12] to help further pin down the physics parameters at threshold. Top is produced symmetrically when produced in the 1S state. The vector coupling of $t\bar{t}$ to the γ and Z can create S- and D-wave resonance states. On the other hand, the axial-vector coupling of the top quark to the Z gives rise to P-wave resonance states. Hence, there is naturally interference between S- and P-waves which gives rise to a forward-backward asymmetry (A_{FB}) proportional to $\beta\cos\theta$. Because of the large width of the resonance states, due to the large Γ_t, these states do overlap to a significant extent, and a sizable A_{FB} develops. The value of A_{FB} varies from about 5% to 12% across the threshold, with the minimum value near the 1S resonance. Since the top width controls the amount of S-P overlap, we expect the forward-backward asymmetry to be a sensitive method for measuring Γ_t.

In summary, a data set of 50 fb^{-1} at threshold would provide sensitivity to m_t and α_s at the level of 120 MeV/c^2 and 0.0025, respectively. Similarly, the sensitivity to the total top decay width is 5–10%. Accelerator and detector designs have become sufficiently stable to make possible calculations which incorporate the systematics associated with luminosity spectra and backgrounds. This would allow better determination of the limiting systematic errors at threshold, which are presently estimated to be at or below the sensitivities above. The measurement of the luminosity spectrum is discussed in more detail in Section 13.

2.3.3 Top Couplings

At the NLC, $e^+e^- \to t\bar{t}$ above threshold will provide a unique opportunity to measure simultaneously all of the top couplings. Due to its rapid weak decay, the top spin is transferred directly to the final state with negligible hadronization uncertainties, therefore allowing the helicity-dependent information contained in the Lagrangian to be propagated to the final state. This final state, expected to be dominated by $bW^+\bar{b}W^-$, can be fully reconstructed with good efficiency and purity, so that a complete helicity analysis can be performed.

The top neutral-current coupling can be generalized to the following expression for the $Zt\bar{t}$ or $\gamma t\bar{t}$ vertex factor:

$$\mathcal{M}^{\mu(\gamma,Z)} = e\gamma^\mu \left[Q_V^{\gamma,Z} F_{1V}^{\gamma,Z} + Q_A^{\gamma,Z} F_{1A}^{\gamma,Z}\gamma^5\right] + \frac{ie}{2m_t}\sigma^{\mu\nu}k_\nu \left[Q_V^{\gamma,Z} F_{2V}^{\gamma,Z} + Q_A^{\gamma,Z} F_{2A}^{\gamma,Z}\gamma^5\right] . \qquad (2.7)$$

This expression reduces to the familiar Standard Model tree level expression when we set the form factors to $F_{1V}^{\gamma} = F_{1V}^{Z} = F_{1A}^{Z} = 1$, with all others zero. The quantities $Q_{A,V}^{\gamma,Z}$ are the usual SM coupling constants: $Q_V^{\gamma} = \frac{2}{3}$, $Q_A^{\gamma} = 0$, $Q_V^Z = (1 - \frac{8}{3}\sin^2\theta_W)/(4\sin\theta_W\cos\theta_W)$, and $Q_A^Z = -1/(4\sin\theta_W\cos\theta_W)$. The non-standard couplings $F_{2V}^{\gamma,Z}$ and $F_{2A}^{\gamma,Z}$ correspond to the electroweak magnetic and electric dipole moments, respectively. While these couplings are zero at tree level in the Standard Model, the analog of the magnetic dipole coupling is expected to attain a value of order α_s/π due to corrections beyond leading order. On the other hand, the electric dipole term violates CP and is expected to be zero in the Standard Model through two loops [18]. Such a non-standard coupling necessarily involves a top spin flip, hence is proportional to m_t.

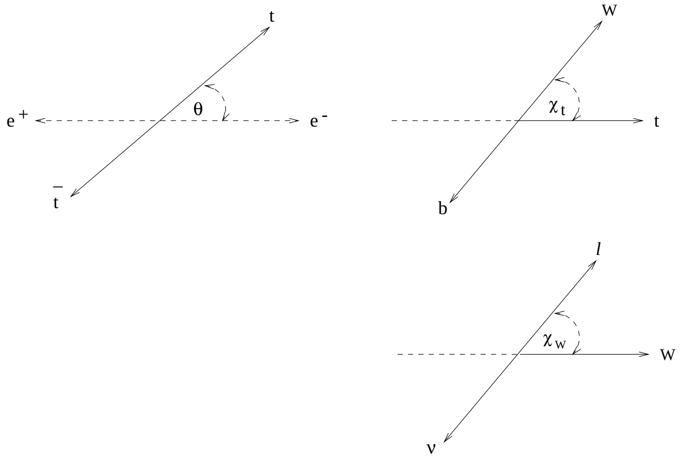

Figure 2.9: Definitions of helicity angles. (a) Production angle θ in $t\bar{t}$ rest frame; (b) χ_t measured in the top rest frame as shown; and (c) χ_W in the W rest frame.

The form factors can be measured through their distinct dependencies on the helicities of the e^-, e^+, t, and $\bar{t}$, which can be accessed experimentally through the beam polarization and the angular distributions in the final state. The production and decay angles can be defined as shown in Fig. 2.9. The angle χ_W is defined in the W rest frame. The analogous statement holds for the definition of χ_t. Experimentally, all such angles, including the angles corresponding to χ_t and χ_W for the $\bar{t}$ hemisphere, are accessible. Given the large number of constraints available in these events, full event reconstruction is entirely feasible. To reconstruct θ one must also take into account photon and gluon radiation. Photon radiation from the initial state is an important effect, which, however, represents a purely longitudinal boost which can be handled within the framework of final-state mass constraints. Gluon radiation can be more subtle. Jets remaining after reconstruction of t and $\bar{t}$ can be due to gluon radiation from t or b, and the correct assignment must be decided based on the kinematic constraints and the expectations of QCD.

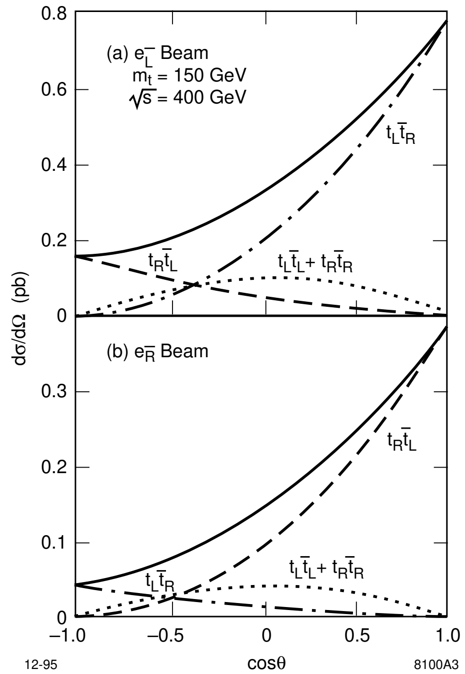

Figure 2.10: Production angle for $t\bar{t}$ for the possible final-state helicity combinations, as indicated, for 100% polarized beams with (a) left-hand polarized electrons, and (b) right-hand polarized electrons. The complete cross sections are the solid curves.

The distributions of the production angle θ for the SM in terms of the various helicity states are given in Fig. 2.10 for left and right-hand polarized electron beam. We see, for example, that for a left-hand polarized electron beam, top quarks produced at forward angles are predominantly left handed, while forward-produced top quarks are predominantly right handed when the electron beam is right-hand polarized. These helicity amplitudes combine to produce the following general form for the angular distribution [19]:

$$\frac{d\sigma}{d\cos\theta} = \frac{\beta_t}{32\pi s}\left[c_0 \sin^2\theta + c_+(1+\cos\theta)^2 + c_-(1-\cos\theta)^2\right] , \tag{2.8}$$

where c_0 and $c_\pm$ are functions of the form factors of Eq. 2.7, including any non-standard couplings. The helicity structure of the event is highly constrained by the measurements of beam polarization and production angle.

For the measurement of the decay form factors, there are two alternative methods that might provide higher statistics. The first is to measure the top quark decay distributions using polarized beams at the $t\bar{t}$ threshold, making use of the fact that the spin of the nonrelativistic top quarks follows the spin of the incident electron and positron [20]. The second is to analyze the polarization of top quarks above threshold using the beam axis boosted to the top frame; this gives a very high polarization for the decay analysis [21].

For the top charged-current coupling we can write the Wtb vertex factor as

$$\mathcal{M}^{\mu,W} = \frac{g}{\sqrt{2}}\gamma^\mu \left[P_L F_{1L}^W + P_R F_{1R}^W\right] + \frac{ig}{2\sqrt{2}\, m_t}\sigma^{\mu\nu}k_\nu \left[P_L F_{2L}^W + P_R F_{2R}^W\right], \tag{2.9}$$

where the quantities $P_{L,R}$ are the left-right projectors. In the Standard Model, we have $F_{1L}^W = 1$ and all others zero. The form factor F_{1R}^W represents a right-handed, or $V + A$, charged current component. As mentioned earlier, the case where the W is longitudinally polarized is particularly relevant for heavy top, and the χ_t and χ_W distributions are sensitive to this behavior.

We now outline an analysis [22] to measure or set limits on the various form factors mentioned above. We consider a modest integrated luminosity of 10 fb^{-1}, $m_t = 180$ GeV/c^2, and $\sqrt{s} = 500$ GeV. Electron beam polarization is assumed to be $\pm 80\%$. The decays are assumed to be $t \to bW$. In general, one needs to distinguish t from $\bar{t}$. The most straightforward method for this is to demand that at least one of the W decays be leptonic, and to use the charge of the lepton as the tag. (One might imagine using other techniques, for example with topological secondary vertex detection one could perhaps distinguish b from $\bar{b}$.) So we assume the following decay chain:

$$t\bar{t} \to b\bar{b}WW \to b\bar{b}q\bar{q}'\ell\nu, \tag{2.10}$$

where $\ell = e, \mu$. The branching fraction for this decay chain is 29%.

Since the top production and decay information is correlated, it is possible to combine all relevant observables to ensure maximum sensitivity to the couplings. In this study, a likelihood function is used to combine the observables. We use the Monte Carlo generator developed by Schmidt [23], which includes $t\bar{t}(g)$ production to $\mathcal{O}(\alpha_s)$. Most significantly, the Monte Carlo correctly includes the helicity information at all stages. The top decay products, including any jets due to hard gluon radiation, must be correctly assigned with good probability. The correct assignments are rather easily arbitrated using the W and top mass constraints. When the effects of initial-state radiation and beamstrahlung are included, it has been shown [19] that the correct event reconstruction can be performed with an efficiency of about 70%. The overall efficiency of the analysis, including branching fractions, reconstruction efficiency, and acceptance, is about 18%.

After simple, phenomenological detection resolution and acceptance functions are applied, the resulting helicity angles (see Fig. 2.9) are then used to form a likelihood which is the square of the theoretical amplitude for these angles given an assumed set of form factors. Table 2.3 summarizes some of the results of this analysis. The upper and lower limits of the top quark couplings in their departures from the Standard Model values are given at 68% and 90% CL. All couplings, with real and imaginary parts, can be determined in this way. The right-handed charged-current coupling is shown both for unpolarized and 80% left-polarized electron beam, whereas the other results assume 80% left-polarized beam only. We see that even with a modest integrated luminosity of 10 fb^{-1} at $\sqrt{s} = 500$ GeV, the sensitivity to the form factors is quite good, at the level of 5–10% relative to Standard Model couplings. In terms of absolute units, the 90% CL limit of F_{2A}^Z at 0.15, for example, corresponds to a t-Z electric dipole moment of 8×10^{-18} e-cm.

Table 2.3: Results from the global top quark form factor analysis described in the text, for a data sample of 10 fb^{-1} and $\sqrt{s} = 500$ GeV.

Form Factor	SM Value (Lowest Order)	Limit 68% CL	Limit 90% CL
$F_{1R}^W(P=0)$	0	± 0.13	± 0.18
$F_{1R}^W(P=80\%)$	0	± 0.06	± 0.10
F_{1A}^Z	1	1 ± 0.08	1 ± 0.13
F_{1V}^Z	1	1 ± 0.10	1 ± 0.16
F_{2A}^γ	0	± 0.05	± 0.08
F_{2V}^γ	0	± 0.07	${}^{+0.13}_{-0.11}$
F_{2A}^Z	0	± 0.09	± 0.15
F_{2V}^Z	0	± 0.07	± 0.10
$\Im(F_{2A}^Z)$	0	± 0.06	± 0.09

2.3.4 The Higgs-Top Yukawa Coupling

The coupling strength of the Higgs boson to a fermion is proportional to the fermion's mass. The Higgs-top coupling is consequently large and may be unique among the Higgs-fermion couplings in that it is accessible to direct measurement. Such measurements have been contemplated at LHC [24], but they require efficient vertex tagging in high-luminosity running. The environment at NLC is much cleaner, but the luminosity requirements are comparable. With the availability of large data sets (> 50 fb^{-1}), several approaches are tractable at NLC: (1) for light to moderate mass Higgs bosons, the $t\bar{t}$ production cross-section near threshold is sensitive to the Higgs contribution to the $t\bar{t}$ potential; (2) for relatively light Higgs, the yield of $t\bar{t}H$ events measures the Higgs-top coupling; and (3) for Higgs masses exceeding the $t\bar{t}$ threshold, the Higgs boson resonance can appear in $t\bar{t}Z$ events and exhibit the Higgs-top coupling.

Threshold measurements have been discussed above for their intrinsic interest and sensitivity to basic top parameters. Here we note that the presence of an additional attractive, short range force arising from Higgs exchange increases the modulus of the toponium wave-function at the origin, and thereby enhances the cross-section. Fig. 2.11 shows the distinctive energy dependence of the Higgs enhancement factor, which peaks at the 1S state [25]. Fujii *et al.*[12] have simulated a threshold scan of 10 points, spaced at 1 GeV intervals, to de-

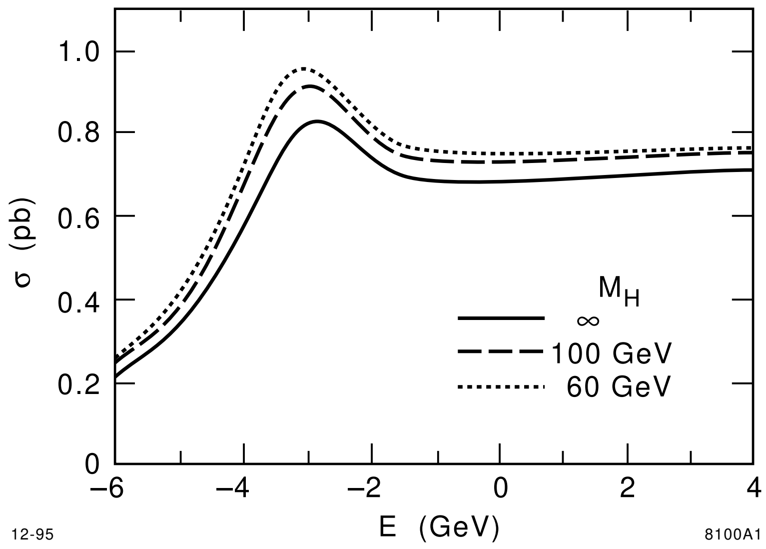

Figure 2.11: Theoretical cross section as a function of Higgs mass for $m_t = 180$ GeV/c^2.

termine the sensitivity to the Higgs-top coupling strength. Their results imply that a 10% measurement is possible with 100 fb^{-1} evenly distributed over the 10 points for $M_H = 100$ GeV. The enhancement is roughly inversely proportional to the Higgs mass, so the scan would yield a 20% (30%) measurement for a 200 (300) GeV Higgs mass. An optimized scan will do better.

The $t\bar{t}H$ events almost always result from "Higgs-strahlung", radiation of the Higgs boson from one of the top quarks, so their yield provides a measure of the square of the Higgs-top coupling. The cross-section for the process is small [26], in the $\mathcal{O}(1)$ fb range for a 500 GeV NLC and $M_H < 100$ GeV. Detection of the events is challenging; they typically contain 8 jets, including 4 b jets. The process $e^+e^- \to t\bar{t}Z$ occurs at comparable rate, and along with $e^+e^- \to t\bar{t}jj$ constitutes the important background. Preliminary studies [12, 27] show that a 100 fb^{-1} sample at 500 GeV will give a $\leq 15\%$ measurement of the Higgs-top coupling for $M_H \leq 100$ GeV. At $\sqrt{s} = 1000$ GeV, the sensitivity extends to over 200 GeV for a measurement of similar accuracy.

The cross-section for $e^+e^- \to t\bar{t}Z$ is about 5 fb between 500 and 1000 GeV center-of-mass energies. When the Higgs mass is above the $t\bar{t}$ threshold, this cross section is enhanced by the process $e^+e^- \to Z^0H^0$, with Higgs decay to $t\bar{t}$. Fujii *et al.* [28] have studied the process for $m_t = 130$ GeV, and concluded that, with an integrated luminosity of 60 fb^{-1} at $\sqrt{s} = 600$ GeV, one could measure the top-Higgs coupling within 10% for a 300 GeV Higgs. For Higgs masses above $2m_t$, the cross-section is lower, and the increased width of the Higgs will make isolating a signal in the $t\bar{t}$ invariant mass distribution more difficult. Even so, one could measure the Higgs-top coupling for a 400 GeV Higgs produced at $\sqrt{s} = 1000$ GeV within about 35% with a data sample of 100 fb^{-1}.

The Higgs-strahlung process is also sensitive to deviations from the Standard Model involving extended Higgs sectors. The $t\bar{t}H$ final state can result from Higgs emission from the t (or $\bar{t}$), or from the intermediate Z. Interference between these sub-processes can give rise to large CP violating effects in extended Higgs models. This was studied in Ref. [29] for a range of two-Higgs doublet models, and it was found that for roughly 100 fb^{-1} of data at $\sqrt{s} = 800$ GeV it would be possible to observe a significant CP asymmetry in a number of final-state observables.

The Higgs-top coupling can be determined in the case that the Higgs is very heavy ($M_H > 400$ GeV/c^2) by measuring the rate of the process $e^+e^- \rightarrow \nu\bar{\nu}t\bar{t}$ At $\sqrt{s} = 1500$ GeV, the cross section for this process is about 2 fb in the absence of a Higgs, but will be enhanced by more than a factor of two for Higgs masses in the range 400–1000 GeV/c^2. Preliminary studies by Fujii [28] show that care is required to eliminate radiative $t\bar{t}$, $e^+e^-t\bar{t}$, and $t\bar{t}Z$ backgrounds, but suggest that the Higgs-top coupling can be measurable up to $m_H = 1$ TeV/c^2. The case of a very heavy Higgs boson is discussed in more detail in Section 7.3.

2.3.5 Top Physics Reach of NLC and Hadron Colliders

Table 2.4 summarizes the top physics reach of the NLC and several hadron colliders. The Tevatron Upgrade (TeV*) will establish the baseline for top quark physics in the LHC/NLC era, and will address many subjects of interest in top physics. Its reach has been studied in a report by Amidei *et al.* [30]. The Atlas TDR [24] provides some information on the top physics reach at LHC; this subject will certainly be developed further in the future. The table at best represents what has been studied to date. If a particular measurement at a particular machine has not yet been analyzed, the corresponding entry has been left blank. An "X" marks measurements that cannot be made at a particular machine, by virtue of excessive backgrounds, insufficient signal, or unavailable production mechanisms.

The table demonstrates how crucial a role the NLC plays in obtaining a complete picture of top quark physics. NLC will provide the definitive top mass measurement. It will provide the only direct measure of the top width; at hadron colliders, the total width can be inferred only from a V_{tb} measurement using the assumption that the top has no unobserved exotic decays. The NLC will measure the axial-vector and vector electroweak couplings, some of the charged-current couplings (expressed here as CKM elements), the top-Higgs coupling, and the flavor specific strong coupling. Hadron colliders will also measure the charged current couplings (although V_{td} is probably impossible at both hadron and e^+e^- colliders), and the strong and electromagnetic couplings, but not the couplings to the Z. The LHC may probe the top-Higgs coupling by isolating $t\bar{t}H$ events, but only with difficulty. The NLC can measure the top decay form factors, checking for longitudinal W production and searching for right-handed W's, as can the hadron colliders. Only the NLC can measure the electroweak magnetic and electric dipole moments, because they depend on the neutral current production mechanism. We should note that LHC can be sensitive to top-associated CP violation through more complicated effective interactions [31, 32]. Rare decays with distinctive signatures can be sought in either environment, with the advantage to hadron

Table 2.4: Top Physics at Future Facilities

Quantity	TeV* (1 fb^{-1})	TeV33 (10 fb^{-1})	LHC (100 fb^{-1})	NLC($\sqrt{s}=360$) (50 fb^{-1})	NLC($\sqrt{s}=500$) (50 fb^{-1})
Δm_t	3.5 GeV/c^2	2.0 GeV/c^2	2 GeV/c^2	0.20 GeV/c^2	
$\Delta\Gamma_t$				6–8%	
Δa_t	X	X	X		4%
Δv_t	X	X	X		5%
ΔV_{tb}	14%	6%	X		
ΔV_{ts}	X	X	X?	?	?
ΔV_{td}	X	X	X	X	X
$\Delta\lambda_t$	X	X	?	14%	20%
$\Delta\alpha_s^t$	$(\sigma_{t\bar{t}}=11\%)$	$(\sigma_{t\bar{t}}=4\%)$		0.005	
$\Delta B(t\to bW^0)$	4%	1.3%		1%	
$\Delta B(t\to bW_R)$	2%	0.6%			2%
$\Delta\delta$	X	X	X		$< 0.3\, e\hbar/2m_t$
Δd	X	X	X		$< 4\times 10^{-18}$ e-cm
$B(t\to H^+b)$	$< 15\%$	$< 6\%$	$< 1.4\%$		$< 2\%$
$B(t\to\tilde{t}\tilde{\chi}^0)$					$< 1\%$
$B(t\to c\gamma)$	$< 0.3\%$	$< 0.04\%$			
$B(t\to cZ)$	$< 1.5\%$	$< 0.4\%$	$< 5\times 10^{-5}$		$<$ few $\cdot 10^{-4}$
$B(t\to ch^0)$				$< 1\%$	

decays by virtue of the large statistical samples anticipated. The more exotic decays, *e.g.* $t\to\tilde{t}\tilde{\chi}^0$, are more sensitively sought in the clean environment of the NLC.